RESEARCH ARTICLE

Encapsulation of *Tinospora cordifolia* plant in Ni-doped TiO_2 nanoparticles for the degradation of malachite green dye

Article history:
Received: 21-03-2023
Revised: 08-08-2023
Accepted: 25-07-2023

Naveen Thakur[a], Nikesh Thakur[b], Kuldeep Kumar[c], Vedpriya Arya[d], Ashwani Kumar[e]

Abstract: The primary global source of water pollution is textile dyes. Highly stable organic dyes are produced by these industries that are released untreated into nearby ponds, lakes, and rivers. This paper is devoted to the synthesis of the nickel-doped anatase phase of TiO_2 nanoparticles (Ni-ATD NPs) by encapsulating plant *Tinospora cordifolia* through a microwave-assisted method for degradation of malachite green dye. The synthesized NPs were calcinated at 400 °C temperature to achieve the anatase phase. The synthesized Ni-ATD NPs were analyzed with different characterization methods. X-ray diffraction and Raman analysis confirmed the crystalline nature of Ni-ATD NPs with a tetragonal structure having a crystallite size of 11 nm. Scanning electron microscope determined the spherical surface morphology for synthesized NPs. The absorption peaks of Ni-ATD NPs were originated from 360 to 370 nm from UV-visible spectroscopy in which the bandgap was found to be 3.45 eV. The photocatalytic activity for MG dye was evaluated under ultra-violet light using Ni-ATD NPs for 90 min which exhibited a degradation of up to 100%.

Keywords: malachite green; *Tinospora cordifolia;* titanium dioxide.

[a] Department of Physics, Career Point University, Hamirpur, Himachal Pradesh 176041, India. Centre for Nano-Science and Technology, Career Point University, Hamirpur, Himachal Pradesh 176041, India. naveenthakur2327@gmail.com Corresponding author.

[b] Department of Physics, Career Point University, Hamirpur, Himachal Pradesh 176041, India. Centre for Nano-Science and Technology, Career Point University, Hamirpur, Himachal Pradesh 176041, India.

[c] Department of Chemistry, Career Point University, Hamirpur, Himachal Pradesh 176041, India. Centre for Nano-Science and Technology, Career Point University, Hamirpur, Himachal Pradesh 176041, India.

[d] Patanjali Herbal Research Department, Patanjali Research Institute, Haridwar, Uttarakhand 249405, India.

[e] Patanjali Herbal Research Department, Patanjali Research Institute, Haridwar, Uttarakhand 249405, India.

1. INTRODUCTION

With the success of contemporary companies, particularly those that deal with textile dyes, a significant problem with the acquisition of fresh water has arisen due to the massive amounts of wastewater and other types of effluents that are emitted (Sudha & Sivakumar, 2015; Khatana *et al.*, 2021; Anu, Thakur & Kumar, 2018). Pollution of organic dyes is a major issue that the world is facing today, including the scarcity of reliable and pure natural energy and environmental hazards. These pollutant dyes can easily disrupt and ruin the ecological balance that will detrimentally affect all living things including people and plants (Thakur *et al.*, 2021a, 2022a; Kumar *et al.*, 2022a). Therefore, there is a pressing need to develop some useful procedures that can turn dangerous and deadly pollutants into harmless ones (Sathiyan *et al.*, 2020; Balkrishna *et al.*, 2021a, 2021b). The influence of nano-photocatalysts is recognized as the best for addressing the energy problem, while dye treatment nano-photocatalysts are seen as the most successful at controlling environmental damage issues (Thakur *et al.*, 2021a, 2022b; Kumar *et al.*, 2021). These nano-catalysts have good conversion capabilities from photons energy to natural energy, which is advantageous for the breakdown of the principal hazardous organic pollutants (Mostakhdemin *et al.*, 2020; Sharma *et al.*, 2021a,

2021c). Titanium dioxide (TiO_2) has been demonstrated to be the most effective potent oxidizing and catalyst agent due to its initial application in heterogeneous photocatalysis under UV light (Krishnan *et al.,* 2022; Kumar *et al.,* 2020a, 2022b, 2023a).

TiO_2 is classified into three crystal structures namely Anatase, Rutile, and Brookite. The anatase phase exhibits extremely high photocatalytic characteristics due to its greater surface area and wide optical bandgap (3.0-3.7 eV) when exposed to light with wavelengths of 380 nm and this exposure causes the formation of electrons-holes pairs in redox reactions (Thakur *et al.,* 2021a, 2021b, 2023a). Numerous organic compounds can be oxidized in aqueous solutions by the reactive oxygen species (ROS) generated by TiO_2 under the influence of UV light (Nithya *et al.,* 2018). Doping in TiO_2 with various transition metals (e.g., Fe, Cu, Ni, Cr, Pt) can enhance the photocatalytic activity under the influence of UV light (Suwarnkar *et al.,* 2014; Anu *et al.,* 2020; Thakur *et al.,* 2020). Under UV light, doping-induced bandgap narrowing allows TiO_2 to become more effective catalytic and creates a large number of ROS. Charge recombination, or an intermediate energy level between the conduction and valence bands, is prevented by changes in lattice properties or dopants acting as electron traps (Zhao *et al.,* 2018; Patial & Thakur, 2018; Kumar *et al.,* 2020b).

The green approach leads to nanoparticles (NPs) unique chemical and physical properties due to larger area with respect to volume compared to bulk material with the same composition. It also allows to use as catalysis for the degradation of organic dyes, drug delivery, anticancer, antibacterial, and many more applications (Kubiak *et al.,* 2020). The green method can manage the morphology (shape and size) of NPs like nanorods, nanospheres, nanoporous, and nanowires, which plays an important role in a number of emerging applications. *Tinospora cordifolia* (TC), also known as *"Guduchi"* in Sanskrit and a member of the Menispermaceae family, is found at higher elevations. The male flower is grouped into racemose panicles whereas the female flower is solitary (Parthipan, Aravindhan & Rajendran, 2011). Alkaloids, steroids, di-terpenoid lactones, aliphatic compounds, and glycosides are just a few of the active substances that have been reported to be isolated from the plant's body, including the root and stem. Traditional Ayurvedic medicine has long utilized TC to treat several conditions including skin diseases, chronic diarrhea, jaundice, cancer, bone fractures, asthma, deadly bug bites, and eye issues (Upadhyay *et al.,* 2010).

TiO_2 is considered as a promising photocatalyst that is used for the degradation of inorganic as well as organic dyes in wastewater due to its biological as well as chemical stability. The present work studies the synthesis of the nickel-doped anatase phase of TiO_2 (Ni-ATD) NPs by encapsulating plant TC through a microwave-assisted method for the degradation of malachite green (MG) dye. MG is an organic substance utilized in the pigment industry as well as the dyestuff industry as a triarylmethane dye. MG technically refers to the chloride salt $[C_6H_5C(C_6H_4N(CH_3)_2)_2]Cl$, although the phrase is frequently used to simply refer to the colored cation as shown in Figure 1.

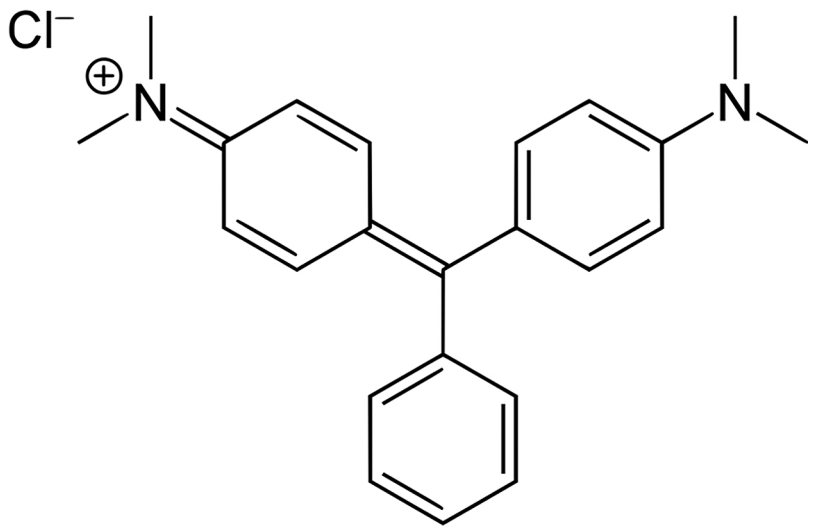

Figure 1. Chemical structure f malachite green dye.

2. MATERIALS AND METHODS

2.1. Materials

Chemical	Chemical formula	Molecular mass (g/mol)	Supplier	Purity[a] (%)
Titanium (IV) Isopropoxide (TTIP)	$Ti(OCH(CH_3)_2)_4$	284.22	Sigma Aldrich	97
Nickle (II) chloride hexahydrate	$NiCl_2.6H_2O$	237.7	Emplura	98.5
Ammonia	NH_3	17.031	Emplura	25
Ethanol (analytical reagent)	C_2H_5OH	46.07	Sigma Aldrich	99.9
Malachite green	$C_{23}H_{25}ClN_2$	364.911	Merck	—
[a] Declared by the supplier.				

Table 1. List of the chemicals with description.

2.2. Methods

2.2.1. Extract of stems of TC plant

In the Himachal Pradesh district of Hamirpur, local locations were used to collect the fresh stems of the TC plant. To get rid of any pollutants that might have been on the stems, the collected stems were properly cleaned with distilled water. The cleaned stems weighed exactly 5 g. The stems were broken and sliced into little pieces. Additionally, 50 ml of distilled water was used to boil well-minced stems for 25-30 min at 70-80 °C. The assembly consists of the attachment of the condenser with the round bottom flask standing on the rota-mantle with constant stirring. Further, the boiled extract was filtered and used for the synthesis of Ni-ATD NPs.

2.2.2. Green synthesis of Ni-ATD NPs

By using the microwave-assisted method, Ni-ATD NPs were synthesized via encapsulating plant TC. 0.01 M solution of TTIP was mixed in ethanol with constant stirring on the magnetic stirrer for 30 min. 0.1% of Ni metal salt ($NiCl_2{\cdot}6H_2O$) was dissolved in 6 ml ethanol and added to the above TTIP solution. 6 ml of plant TC extract was added to a mixture of TTIP and Ni solution. To this reaction mixture, 6 ml of ammonia was added drop-by-drop and stirred for 30 min. The obtained solution was kept in the domestic microwave oven having temperature from 150 to 300 °C with an operating frequency of 2.45 GHz and power of 700 W for 2 min. After treating in the microwave, the obtained Ni-ATD NPs were centrifuged with distilled water and ethanol for 3-4 times at 6000-8000 rpm for 5 min. Further, these NPs were dried in a vacuum oven at a pressure of 5 KPa at 70 °C temperature for 2 h. After drying in a vacuum oven, the NPs were calcinated at 400 °C temperature in a muffle furnace for 2 h to acquire the anatase phase. The synthesis approach was performed in triplet and the synthesis yield was (mass by mass%) found to be 43 ± 0.75%.

2.3. Material characterizations

Ni-ATD NPs crystal structure and crystallite size were investigated using X-ray diffraction (XRD). The crystal phase analysis of synthesized Ni-ATD NPs was done by using Raman spectroscopy. The UV-visible spectrophotometer was used to measure the bandgap of NI-ATD NPs. Scanning electron microscope (SEM) was used to measure the surface morphology of Ni-ATD and also elemental analysis has been carried out by using the Energy-dispersive X-ray spectroscopy (EDS) attached to the SEM micrograph. Transmission electron microscopy (TEM) was used to examine the particle size of synthesized Ni-ATD NPs.

2.4. Photocatalytic activity

The photocatalytic activity was examined for the degradation of MG dye by using Ni-ATD NPs. The synthesized Ni-ATD NPs were injected in 10 ppm of MG dye under UV light (Mercury-vapor lamp of 125 W) with a wavelength of 360-380 nm. In a dark chamber, a UV lamp was positioned vertically with an average distance of 20 mm above the reaction mixture. 10, 25 & 50 mg of Ni-ATD NPs were dissolved in a 100 ml aqueous solution of dye and kept in UV chamber for 90 min. By using a UV-visible spectrophotometer, the rate of degradation was monitored at intervals of 15 min and a change in

absorbance was observed at wavelength, λ = 624 nm. The photocatalytic experiment was performed in triplicate to ensure the precision of the study.

3. RESULTS AND DISCUSSION

3.1. XRD analysis

The XRD pattern of synthesized Ni-ATD NPs is shown in Figure 2. The intense peaks corresponding to miller indices *(hkl)* of Ni-ATD NPs are 25.36°, 37.83°, 48.13°, 53.96°, 55.11°, 62.16°, 69.38°, 70.22°, and 75.29° with respect to (101), (004), (200), (105), (211), (204), (116), (220), and (215), respectively. JCPDS card numbers 21-1272 (Santhi *et al.*, 2020) confirmed the Ni-ATD NPs have tetragonal structures that are validated by the peaks of XRD patterns as shown in Figure 2. There was no sign of any Ni oxide or Ni composites regardless amount of substituted Ni in the TiO_2 crystal lattice. The crystallite size (D) and % crystallinity of synthesized Ni-ATD NPs was found to be 11 nm and 97% by using equations (1) and (2), respectively (Johari *et al.*, 2019). So, a highly intense peak indicates the higher crystallinity of synthesized NPs which is more favorable for photocatalytic activity because higher crystallinity decreases the amount of trapping that assists the recombination of electron-hole pairs (Santhi *et al.*, 2020).

$$D = \frac{K\lambda}{\beta \, Cos\, \theta} \quad (1)$$

$$\%\ crystallinity = \frac{Area\ of\ crystalline\ peaks}{Area\ of\ all\ peaks} \quad (2)$$

where *K:* Scherrer constant
λ: Wavelength
β: Full-width half maxima
θ: Bragg's angle

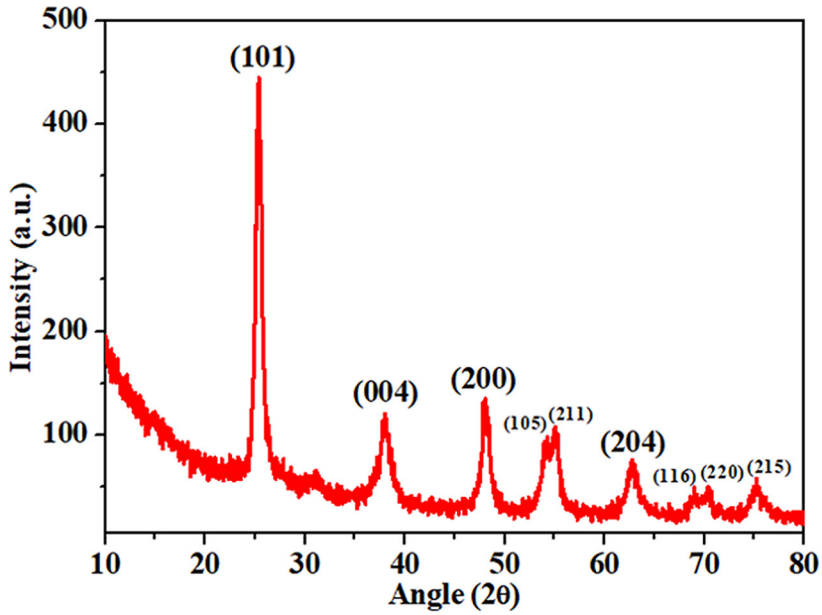

Figure 2. X-ray diffraction peaks of synthesized Ni-ATD NPs.

3.2. Raman analysis

Raman spectroscopy was used to study the crystalline structure of Ni-ATD NPs that were calcinated at temperatures 400 °C with frequencies between 100 and 900 cm^{-1}. Figure 3 represents the Raman peaks of synthesized Ni-ATD NPs. The peaks corresponding to vibrational modes are 145, 197, 397, 516, and 640 cm^{-1} with respect to E_g, E_g, B_{1g}, $A_{1g} + B_{1g}$, and E_g, respectively. The Raman peaks supported Ni-ATD NPs with their well-crystallized state which are in good accordance with the XRD findings displayed in Figure 3. It is observed that there is a shifting of Raman peaks towards a higher wavenumber because of modification in the bond length of molecules due to the bond length of molecules (Phytocompounds) present in plant TC is low (Liu *et al.*, 2015). Thus, the high crystallinity of synthesized NPs correlates with the higher photocatalytic performance of organic dyes (Wang *et al.*, 2015).

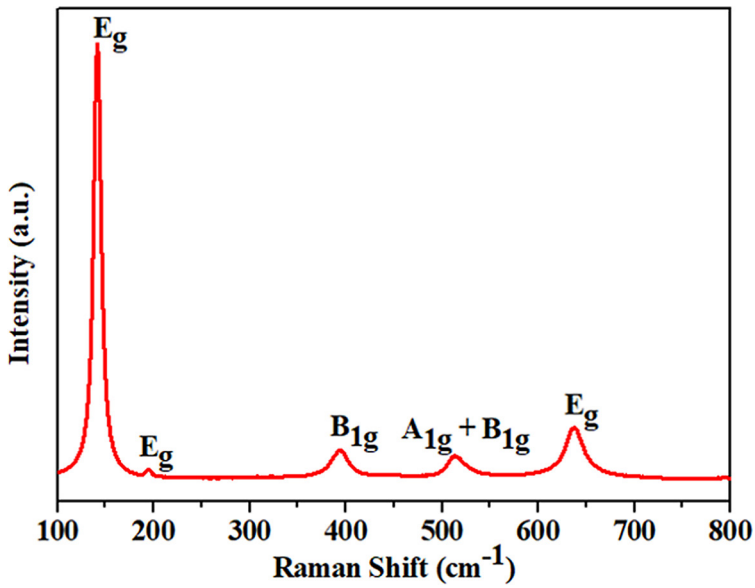

Figure 3. Raman spectra of synthesized Ni-ATD NPs.

3.3. UV analysis

The bandgap of synthesized N-ATD NPs was determined by UV-visible spectroscopy in the range of 200-700 nm. Figure 4 determined that with the addition of Ni in the precursor solution of Titanium, the absorption peaks were shifted from 360 to 370 nm. The bandgap of Ni-ATD NPs was found to be 3.45 eV using equation (3) (Sharma *et al.*, 2020a, 2020b), which is favorable to produce electron-hole pairs under the UV light. The absorbance can change based on several variables, including particle size, oxygen deprivation, imperfections in the synthesized material, etc (Wang *et al.*, 2015). The sp-d exchange interactions between band electrons and localized d electrons of the Ni^{2+} ions substituting Ti^{4+} cations can be used to explain a modest shift in the absorbance of Ni-ATD NPs (Johari *et al.*, 2019). The valence band edge changed downward and the conduction band edge changed upward as a result of the interactions between the p-d and s-d exchange, increasing the band gap. These structure variations may change mass density and lead to different electronic configurations (Assayehegn *et al.*, 2020).

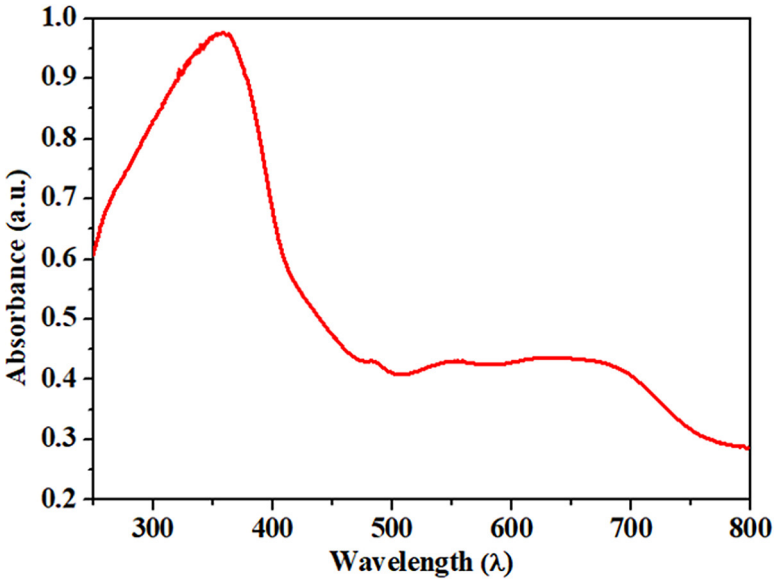

Figure 4. UV spectra of synthesized Ni-ATD NPs.

$$Eg = \frac{hc}{\lambda} \quad (3)$$

where *h:* Planck's constant
c: Speed of light
λ: Wavelength

3.4. SEM-EDS analysis

The surface morphology and elemental analysis of synthesized Ni-ATD NPs were determined by SEM-EDS spectroscopy. Figure 5 represents the SEM-EDS images of Ni-ATD NPs. It shows that Ni-ATD NPs synthesized using the microwave-assisted technique have spherical-like spheroidal shapes. It is evident that adopting a microwave-assisted method for synthesis at a specific temperature, frequency, and power aids helps the metal precursors as well as encapsulated agents for controlling the shape as well as the size of NPs and also it prevents the aggregation during the formation of NPs (Wojnarowicz *et al.*, 2018). According to EDS data, synthesized Ni-ATD NPs are only composed of nickel, titanium, and oxygen. The peaks at 2-3 keV are accredited to carbon as well as oxygen that is found in plant TC.

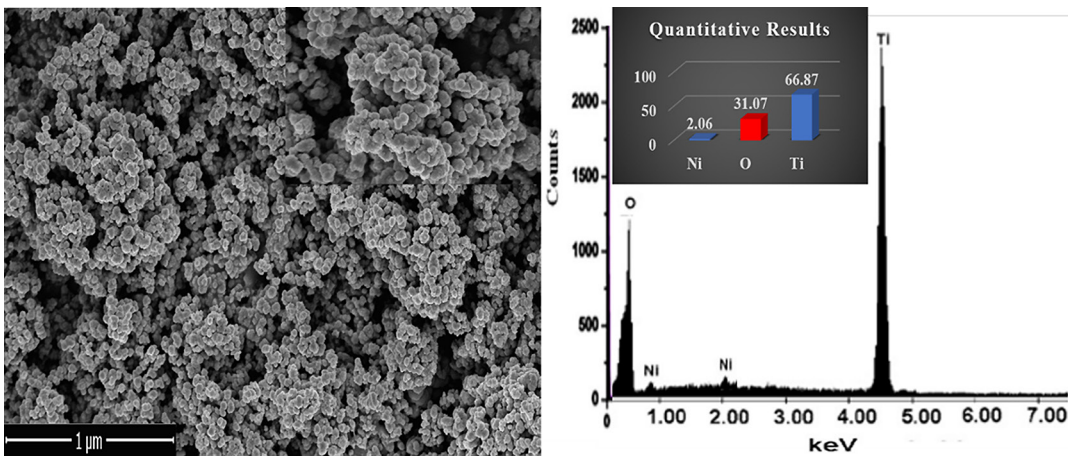

Figure 5. SEM-EDS images of synthesized Ni-ATD NPs.

3.5. TEM analysis

The particle size of synthesized Ni-ATD NPs was examined using TEM spectroscopy. TEM study determines the disparity in the size of Ni-ATD NPs that can be due to the occurrence of several biomolecules present in plant TC. Figure 6 represents the TEM images of synthesized Ni-ATD NPs. It is found that synthesized NPs have a spherical shape with an average particle size of 8 ± 0.50 nm, determined using ImageJ software for 45-50 particles in the image. So it is concluded from here that the green approach synthesized NPs with a small particle size as well as spheroidal shape is more favorable for photocatalytic activity.

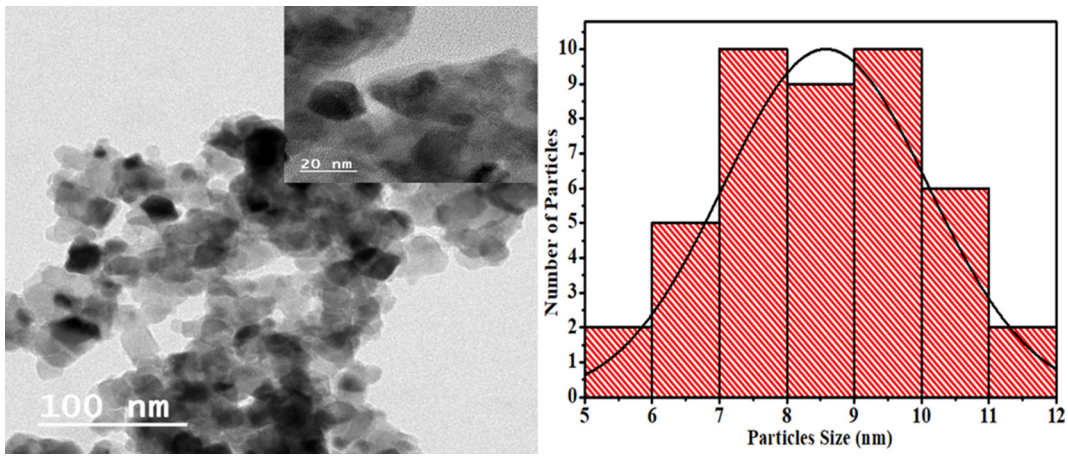

Figure 6: TEM images synthesized Ni-ATD NPs.

4. PHOTOCATALYTIC ACTIVITY

The persuaded photocatalytic process, which is a type of heterogeneous photocatalytic process, oxidizes and depletes the organic molecule through a redox reaction. Energy levels above this bandgap will cause electrons (e^-) to move into the conduction band while keeping h^+ ions at the top of the valence band for the creation of electron-hole pairs in Ni-ATD NPs, which have a forbidden bandgap ranging from 3.2 to 3.7 eV (Li *et al.*, 2020; Thakur *et al.*, 2023b). As the holes are carried toward the surface of the Ni-ATD NPs, the space-charge layer separates the photogenerated electrons and holes.

$$Ni-ATD\ NPs + hv \rightarrow Ni-ATD\ NPs + e^- + h^+$$
$$h^+ + MG \rightarrow MG^{\bullet+}$$
$$e^- + O_2 \rightarrow O_2^{\bullet-}$$
$$h^+ + OH^- \rightarrow OH^{\bullet}$$
$$OH^{\bullet} + MG\ dye \rightarrow intermediate\ product \rightarrow H_2O + CO_2$$
$$O_2^{\bullet-} + MG\ dye \rightarrow intermediate\ product \rightarrow H_2O + CO_2$$

The principal photon energy-derived elements engage with either the adsorbed H_2O or OH^- ions on the surface to produce $^{\bullet}OH$ through a strong oxidation reaction (Mirzaei *et al.*, 2021; Kumar *et al.*, 2023b). Free and active radicals having great oxidizing properties are produced as a result of the reaction. Due to this oxidizing property possessed by them, these radicals are capable of mineralizing the contaminants into small molecules of carbon dioxide. They have an affinity to combine with the water molecules leading to the breakdown of MG dyes (Helmy *et al.*, 2021; Kumar *et al.*, 2023a; Sharma, Kumar & Thakur, 2021b). The photocatalytic degradation of MG dye was evaluated by using synthesized Ni-ATD NPs with different concentrations (10, 25, and 50 mg) in the presence of UV light for 90 min. After 15 min, the absorbance of MG dye was measured with UV-visible spectroscopy at wavelength, λ = 624 nm. The % degradation of MG dye was calculated using equation (4) (Thakur *et al.*, 2021). Figure 7 represents the % degradation of synthesized Ni-ATD NPs. The calculated value of % degradation, standard deviation, and standard error concerning synthesized Ni-ATD NPs are listed in Table 2.

$$\%\ Degradation = \frac{A_o - A}{A_o} \quad (4)$$

where A_o: Absorbance of pure dye
A: Absorbance of the reaction mixture

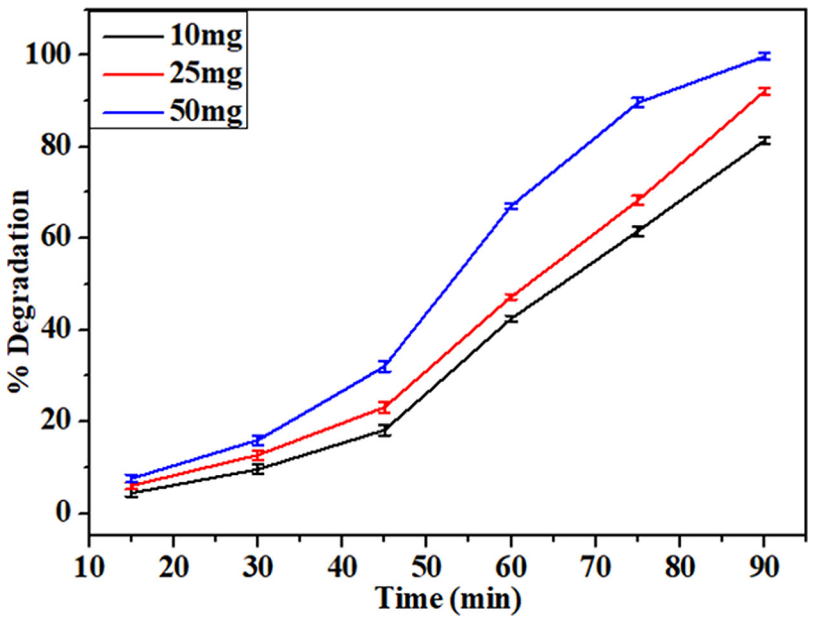

Figure 7. % degradation of synthesized Ni-ATD NPs for MG dye.

From Table 2, it is observed that on increasing the concentration of synthesized Ni-ATD NPs the degradation of MG dye also increases up to 100% because degradation depends upon the proportionality of the catalyst loaded (Pinedo-Escobar *et al.*, 2021). Also, degradation depends upon the size, shape, and bandgap of synthesized NPs which provides active sites as well as the ability

to excite electrons when exposed to UV light (Li *et al.*, 2020). On the analysis of XRD, Raman, UV, SEM-EDS, and TEM spectra, plant TC encapsulated Ni-ATD NPs have small particle size as well as a large bandgap which results in a large generation of more electron holes which provide more surfaces and shorter diffusion path that helps in degradation of MG dye (Pinedo-Escobar *et al.*, 2021). For the photocatalyst to be used in practice, stability is also crucial. As a result, by observing the catalytic activity throughout three cycles of degradation, the cyclic stability of Ni-ATD NPs was examined. The Ni-ATD NPs display a very stable photocatalytic performance without any noticeable deactivation which concluded that after three cycles of testing Ni-ATD NPs exhibit remarkable stability during numerous reuse cycles as shown in Figure 8.

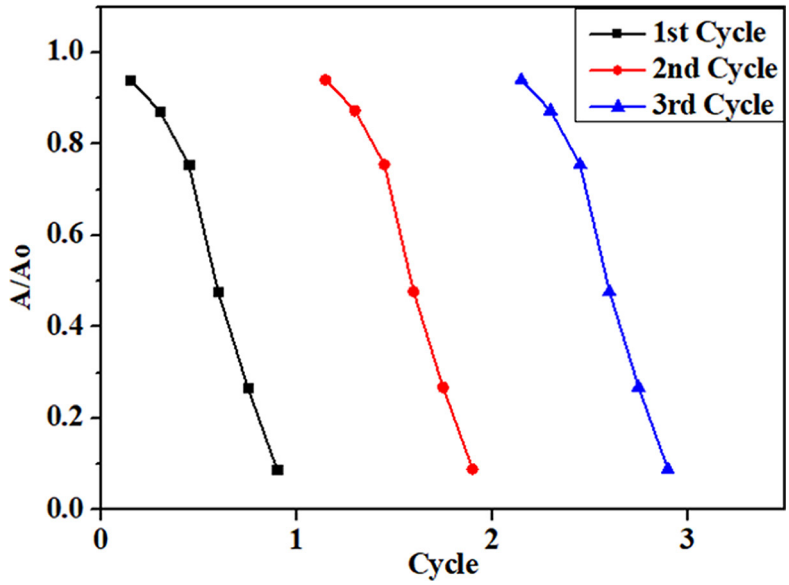

Figure 8. Degradation stability of synthesized Ni-ATD NPs for MG dye.

Concentrations (mg)	Degradation (%)	Standard deviation	Standard error
10	81	0.70946	0.409607
25	92	0.404145	0.233333
50	100	0.152753	0.088192

Table 2. Value of % degradation of synthesized Ni-ATD NPs for MG dye.

5. CONCLUSIONS

The outcomes of the present study revealed that encapsulation of plant TC in Ni-ATD NPs shows a significant influence on the degradation of MG dye. Moreover, results also confirmed that the size and shape of TiO_2 NPs could be controlled by the encapsulation of phytochemicals from a plant. The synthesized Ni-ATD NPs confirmed the high crystallinity with spheroidal shapes which helps in the degradation of MG dye. The rise in the bandgap of Ni-ATD NPs also confirms more generation of electrons holes pairs that help in the degradation of MG dye. Further, the fabrication of plant-encapsulated NPs is very fast, energy-efficient, low-cost, and not toxic to the environment. Therefore, the green approach may be recommended for the industry to synthesize NPs on a wide scale to remove various organic dyes from different wastewaters. These NPs could be used as an antibacterial agent, an anticancer agent, or as a drug-resistant microorganisms. In accumulation, it is also possible to improve medical applications such as bioimaging, bioimplants, drug delivery, treatment of cancer, etc., by manufacturing such non-toxic and cost-effective nano-scale particles.

Acknowledgments

The authors are grateful to the Centre for Nano-Science and Technology in Career Point University, Hamirpur (H.P.) for providing all the necessary facilities to conduct research work. In addition, the authors are grateful to Sophisticated Analytical Instrumentation Facility, Panjab University, Punjab and Sprint Testing Solutions, Mumbai for assistance of characterization of samples.

Conflict of Interest

The authors declare no competing financial interest. ♦

REFERENCES

Anu, Thakur, N., and Kumar, J., 2018. Synthesis and characterization of pure and Zn-doped copper oxide nanoparticles. International Journal of Advance Research in Science and Engineering, 7(8), pp.1-5.

Anu, Thakur, N., Kumar, K. and Sharma, K. K., 2020. Application of Co-doped copper oxide nanoparticles against different multidrug resistance bacteria. Inorganic and Nano-Metal Chemistry, 50(10), pp.933-943.

Assayehegn, E., Solaiappan, A., Chebude, Y. and Alemayehu, E., 2020. Fabrication of tunable anatase/rutile heterojunction N/TiO_2 nanophotocatalyst for enhanced visible light degradation activity. Applied Surface Science, 515, p.145966.

Balkrishna, A., Arya, V., Rohela, A., Kumar, A., Verma, R., Kumar, D., Nepovimova, E., Kuca, K., Thakur, N., Thakur, N. and Kumar, P., 2021a. Nanotechnology Interventions in the Management of COVID-19: Prevention, Diagnosis and Virus-Like Particle Vaccines. Vaccines, 9(10), p.1129.

Balkrishna, A., Kumar, A., Arya, V., Rohela, A., Verma, R., Nepovimova, E., Krejcar, O., Kumar, D., Thakur, N. and Kuca, K., 2021b. Phytoantioxidant Functionalized Nanoparticles: A Green Approach to Combat Nanoparticle-Induced Oxidative Stress. Oxidative medicine and cellular longevity, 2021, pp.1-20.

Helmy, E. T., Abouellef, E. M., Soliman, U.A. and Pan, J. H., 2021. Novel green synthesis of S-doped TiO_2 nanoparticles using Malva parviflora plant extract and their photocatalytic, antimicrobial and antioxidant activities under sunlight illumination. Chemosphere, 271, p.129524.

Johari, N. D., Rosli, Z. M., Juoi, J. M. and Yazid, S. A., 2019. Comparison on the TiO_2 crystalline phases deposited via dip and spin coating using green sol-gel route. Journal of Materials Research and Technology, 8(2), pp.2350-2358.

Khatana, C., Kumar, A., Alruways, M.W., Khan, N., Thakur, N., Kumar, D., and Kumari, A., 2021. Antibacterial Potential of Zinc Oxide Nanoparticles Synthesized using Aloe vera (L.) Burm. f.: A Green Approach to Combat Drug Resistance. Journal of Pure and Applied Microbiology, 15(4), pp.1907-1914.

Krishnan, R., Shibu, S. N., Poelman, D., Badyal, A. K., Kunti, A., Swart, H. C. and Menon, S. G., 2022. Recent advances in microwave synthesis for photoluminescence and photocatalysis. Materials Today Communications, p.103890.

Kubiak, A., Bielan, Z., Kubacka, M., Gabała, E., Zgoła-Grześkowiak, A., Janczarek, M., Zalas, M., Zielińska-Jurek, A., Siwińska-Ciesielczyk, K. and Jesionowski, T., 2020. Microwave-assisted synthesis of a TiO_2-CuO heterojunction with enhanced photocatalytic activity against tetracycline. Applied Surface Science, 520, p.146344.

Kumar, A., Ahmad, S., Chandel, T. and Thakur, N., 2021. Prediction of Intrinsic Spin Half-Metallicity and Ferromagnetism of Co-based Full Heusler Alloys: Hunt for Spintronic Applicability. DAE Solid State Physics Symposium, 55, pp.581-582.

Kumar, A., Chandel, T. and Thakur, N., 2022a. Robust stability, half metallic Ferromagnetism and structural properties of Co2RhSi, and Co2RuSi Heusler compounds-A first principles approach. Materials Today: Proceedings, pp.1-6.

Kumar, A., Singh, S., Sofi, S. A., Chandel, T. and Thakur, N., 2022b. Robustness in half-metallicity, thermophysical and structural properties of Co2YAl (Y= Pd, Ag) Heuslers: a first-principles perspective. Molecular Physics, 120(18), p.2120839.

Kumar, A., Sofi, S. A., Chandel, T. and Thakur, N., 2023a. First-principles calculations to investigate structural stability, half-metallic behavior, thermophysical and thermoelectric properties of Co2YAl (Y= Mo, Tc) full Heusler compounds. Computational and Theoretical Chemistry, 1219, p.113943.

Kumar, A., Thakur, N. and Chandel, T., 2020a. Tuning of electronic energy levels of NH3 passivated ZnO nanoclusters: A first principle study. Computational and Theoretical Chemistry, 1176, p.112743.

Kumar, A., Thakur, N. and Chandel, T., 2020b. Tuning of electronic energy levels of NH3 passivated ZnO nanoclusters: A first principle study. Computational and Theoretical Chemistry, 1176, p.112743.

Kumar, P., Thakur, N., Kumar, K. and Jeet, K., 2023b. Photodegradation of methyl orange dye by using Azadirachta indica and chemically mediated synthesized cobalt doped α-Fe2O3 NPs through co-precipitation method. Materials Today: Proceedings.

Li, R., Yang, J., Xu, S., Zhou, Y., Wang, X., Peng, H. and Du, J., 2020. Preparation of Gd-doped TiO_2 nanotube arrays by anodization method and its photocatalytic activity for methyl orange degradation. Catalysts, 10(3), p.298.

Mirzaei, A., Eddah, M., Roualdès, S., Ma, D. and Chaker, M., 2021. Multiple-homojunction gradient nitrogen doped TiO_2 for photocatalytic degradation of sulfamethoxazole, degradation mechanism, and toxicity assessment. Chemical Engineering Journal, 422, p.130507.

Mostakhdemin, M., Nand, A., Arjmandi, M. and Ramezani, M., 2020. Mechanical and microscopical characterisation of bilayer hydrogels strengthened by TiO_2 nanoparticles as a cartilage replacement candidate. Materials Today Communications, 25, p.101279.

Nithya, N., Bhoopathi, G., Magesh, G. and Kumar, C. D. N., 2018. Neodymium doped TiO_2 nanoparticles by sol-gel method for antibacterial and photocatalytic activity. Materials Science in Semiconductor Processing, 83, pp.70-82.

Parthipan, M., Aravindhan, V. and Rajendran, A., 2011. Medico-botanical study of Yercaud hills in the eastern Ghats of Tamil Nadu, India. Ancient science of life, 30(4), p.104.

Patial, B. and Thakur, N., 2018. Green synthesis of silver nanoparticles using different plants. CPUH-Research Journal, 3(2), pp.40-43.

Pinedo-Escobar, J. A., Fan, J., Moctezuma, E., Gomez-Solís, C., Carrillo Martinez, C. J. and Gracia-Espino, E., 2021. Nanoparticulate double-heterojunction photocatalysts comprising TiO_2 (Anatase)/WO_3/TiO_2 (Rutile) with enhanced photocatalytic activity toward the degradation of methyl orange under near-ultraviolet and visible light. ACS omega, 6(18), pp.11840-11848.

Saranya, K.S., Vellora Thekkae Padil, V., Senan, C., Pilankatta, R., Saranya, K., George, B., Wacławek, S. and Černík, M., 2018. Green synthesis of high temperature stable anatase titanium dioxide nanoparticles using Gum Kondagogu: characterization and solar driven photocatalytic degradation of organic dye. Nanomaterials, 8(12), p.1002.

Sathiyan, K., Bar-Ziv, R., Mendelson, O. and Zidki, T., 2020. Controllable synthesis of TiO_2 nanoparticles and their photocatalytic activity in dye degradation. Materials Research Bulletin, 126, p.110842.

Sharma, S. and Kumar, K., 2021a. Aloe-vera leaf extract as a green agent for the synthesis of CuO nanoparticles inactivating bacterial pathogens and dye. Journal of Dispersion Science and Technology, 42(13), pp.1950-1962.

Sharma, S., Kumar, K. and Thakur, N., 2021b. Green synthesis of silver nanoparticles and evaluation of their anti-bacterial activities: use of Aloe barbadensis miller and Ocimum tenuiflorum leaf extracts. Nanofabrication, 6(1), pp.52-67.

Sharma, S., Kumar, K., Thakur, N. and Chauhan, M. S., 2020a. Ocimum tenuiflorum leaf extract as a green mediator for the synthesis of ZnO nanocapsules inactivating bacterial pathogens. Chemical Papers, 74(10), pp.3431-3444.

Sharma, S., Kumar, K., Thakur, N., Chauhan, S. and Chauhan, M. S., 2020b. The effect of shape and size of ZnO nanoparticles on their antimicrobial and photocatalytic activities: a green approach. Bulletin of Materials Science, 43(1), pp.1-10.

Sharma, S., Kumar, K., Thakur, N., Chauhan, S. and Chauhan, M. S., 2021c. Eco-friendly Ocimum tenuiflorum green route synthesis of CuO nanoparticles: Characterizations on photocatalytic and antibacterial activities. Journal of Environmental Chemical Engineering, 9(4), p.105395.

Sudha, D. and Sivakumar, P., 2015. Review on the photocatalytic activity of various composite catalysts. Chemically Engineering and Processing: Process Intensification, 97, pp.112-133.

Suwarnkar, M. B., Dhabbe, R. S., Kadam, A. N. and Garadkar, K. M., 2014. Enhanced photocatalytic activity of Ag doped TiO_2 nanoparticles synthesized by a microwave assisted method. Ceramics International, 40(4), pp.5489-5496.

https://doi.org/10.37819/nanofab.8.305

Thakur, N., Anu and Kumar, K., 2020. Effect of (Ag, Co) co-doping on the structural and antibacterial efficiency of CuO nanoparticles: A rapid microwave assisted method. Journal of Environmental Chemical Engineering, 8(4), p.104011.

Thakur, N., Kumar, K. and Kumar, A., 2021a. Effect of (Ag, Zn) co-doping on structural, optical and bactericidal properties of CuO nanoparticles synthesized by a microwave-assisted method. Dalton Transactions, 50(18), pp.6188-6203.

Thakur, N., Kumar, K., Thakur, V.K., Soni, S., Kumar, A. and Samant, S. S., 2022a. Antibacterial and photocatalytic activity of undoped and (Ag, Fe) co-doped CuO nanoparticles via microwave-assisted method. Nanofabrication, 7, pp.1-27.

Thakur, N., Thakur, N. and Kumar, K., 2023b. Phytochemically and PVP stabilized TiO_2 nanospheres for enhanced photocatalytic and antioxidant efficiency. Materials Today Communications, 35, p.105587.

Thakur, N., Thakur, N., Bhullar, V., Sharma, S., Mahajan, A., Kumar, K., Sharma, D. P. and Pathak, D., 2021b. TiO_2 nanofibers fabricated by electrospinning technique and degradation of MO dye under UV light. Zeitschrift für Kristallographie-Crystalline Materials, 236(8-10), pp.239-250.

Thakur, N., Thakur, N., Chauhan, P., Sharma, D.P., Kumar, A. and Jeet, K., 2022b. Futuristic role of nanoparticles for treatment of COVID-19. Biomaterials and Polymers Horizon, 1(2), pp.1-22.

Thakur, N., Thakur, N., Kumar, K. and Kumar, A., 2023a. Tinospora cordifolia mediated eco-friendly synthesis of Cobalt doped TiO_2 NPs for degradation of organic methylene blue dye. Materials Today: Proceedings.

Upadhyay, A. K., Kumar, K., Kumar, A. and Mishra, H. S., 2010. Tinospora cordifolia (Willd.) Hook. f. and Thoms.(Guduchi)-validation of the Ayurvedic pharmacology through experimental and clinical studies. International Journal of Ayurveda research, 1(2), p.112.

Wang, X., Kafizas, A., Li, X., Moniz, S. J., Reardon, P. J., Tang, J., Parkin, I. P. and Durrant, J. R., 2015. Transient absorption spectroscopy of anatase and rutile: the impact of morphology and phase on photocatalytic activity. The Journal of Physical Chemistry C, 119(19), pp.10439-10447.

Wojnarowicz, J., Chudoba, T., Gierlotka, S. and Lojkowski, W., 2018. Effect of microwave radiation power on the size of aggregates of ZnO NPs prepared using microwave solvothermal synthesis. Nanomaterials, 8(5), p.343.

Zhao, Q. E., Wen, W., Xia, Y. and Wu, J. M., 2018. Photocatalytic activity of TiO_2 nanorods, nanowires and nanoflowers filled with TiO_2 nanoparticles. Thin Solid Films, 648, pp.103-107